THE JOURNAL OF PHYSICAL CHEMISTRY C

Article

pubs.acs.org/JPCC

Estimating Hybridization of Transition Metal and Oxygen States in Perovskites from O *K*-edge X-ray Absorption Spectroscopy

Jin Suntivich,*[,†,‡,§] Wesley T. Hong,[†,‡] Yueh-Lin Lee,[‡] James M. Rondinelli,[∥] Wanli Yang,[⊥] John B. Goodenough,[#] Bogdan Dabrowski,[○] John W. Freeland,[□] and Yang Shao-Horn*[,†,‡]

[†]Department of Materials Science and Engineering and [‡]Electrochemical Energy Laboratory, Department of Mechanical Engineering, Massachusetts Institute of Technology, Cambridge, Massachusetts 02139, United States

[∥]Department of Materials Science and Engineering, Drexel University, Philadelphia, Pennsylvania 19104 United States

[⊥]Advanced Light Source, Lawrence Berkeley National Laboratory, Berkeley, California 94720, United States

[#]Texas Materials Institute, University of Texas at Austin, Austin, Texas 78712, United States

[○]Department of Physics, Northern Illinois University, DeKalb, Illinois 60115, United States

[□]Advanced Photon Source, Argonne National Laboratory, Illinois 60439, United States

Supporting Information

ABSTRACT: The interaction between the transition metal 3*d* and the oxygen 2*p* states via hybridization underpins many of the phenomena in transition metal oxide materials. We report the empirical trend of this interaction using the pre-edge feature of the O *K*-edge X-ray absorption spectrum. Our assessment method is built on the dipole approximation and the configuration interaction between the transition metal 3*d* and the oxygen 2*p* states. We found that hybridization increases with the number of 3*d* electrons, consistent with the expected electronegativity trend. We support this analysis with density functional calculations, which reveal a systematic increase in the transition metal 3*d* and the oxygen 2*p* state mixing with increasing 3*d*-electron number. Oxidation of the transition metal was also found to increase hybridization, which we believe reflects the reduced transition metal 3*d* and oxygen 2*p* energy difference, causing increased covalency. We compare the analysis from the surface-sensitive electron-yield and the bulk-sensitive fluorescence-yield spectra, revealing that either method can be used to study the hybridization trend. We finally compare and discuss the influence of the lanthanide ions and the influence of the covalency on oxygen electrocatalysis. Our study describes an efficient and simple approach to understand the hybridization trend in transition metal oxides, which has considerable implications for electrochemical energy conversion processes.

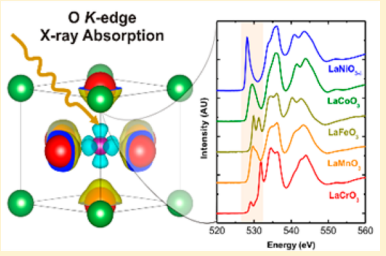

INTRODUCTION

The interaction between the transition metal 3*d* and the oxygen 2*p* states has received substantial attention as a phenomenon underlying many transition metal oxide (TMO) properties, including metal-to-insulator transitions,[1] intercalation potentials,[2,3] and optical[4] and magnetic[5,6] behavior. Active in a variety of TMO crystal families, including perovskites,[1,5−7] spinels,[8] pyrochlores,[9] and layered compounds,[3] the importance of hybridization has been discussed both experimentally and theoretically[10] as an explanation to many bulk and interface effects.[11,12] Recently, hybridization has also been reported to play a critical role in many energy storage technologies, where it appears to decrease lithium intercalation voltages[2,3] and increase the activities of oxygen electrocatalysts.[13,14]

Oxygen 1*s* ("O *K*-edge") X-ray absorption spectroscopy (XAS)[15,16] is one technique that can reveal the hybridization of the transition metal and the oxygen states in oxides. More specifically, the O *K*-edge XAS takes advantage of the first-order transition from the O 1*s* to O 2*p* state to selectively measure the density of unoccupied states with O 2*p* symmetry ("O 2*p* holes").[15,17] This selective excitation is a result of the dominating dipole transition matrix elements, which obey a selection rule of $\Delta l = \pm 1$, so only the unoccupied states with O 2*p* character are probed in the measurement. Therefore, the spectral intensity can reveal the fraction of O 2*p* character that mixes with transition metal 3*d* states (and, thus, the electron sharing between O 2*p* and transition metal 3*d* states).

This advantage of the O *K*-edge XAS has been utilized by de Groot et al.,[15] whose work has related the prepeaks near the threshold of the O *K*-edge XAS collected from a number of binary oxides to the hybridization between O 2*p* and transition metal 3*d* states. Unfortunately, the oxides examined in that study contained different transition metal valence states and/or crystal structures. This leads to ambiguities in assessing the influence of the valency of a given transition metal ion and the number of *d*-electrons for a given valency on the hybridization. Comparing early transition-metal oxides of higher metal valency with late-transition-metal oxides of lower valency, the authors report that the lower prepeak intensities reflect the diminishing hybridization with the number of *d*-electrons. This

Received: October 28, 2013
Revised: January 6, 2014
Published: January 8, 2014

trend is in contrast to the findings from X-ray photoemission spectroscopy studies of transition metal oxides and sulfides.[18,19] In these studies, the charge-transfer gap has been found to decrease with minimal change in the transfer integral, which suggests *increasing* hybridization in going from the earlier to the later of the transition metal series. This motivates the need for more systematic investigation of the chemical trends in metal−oxygen hybridization.

We report a comparison of the degree of transition metal 3*d*−O 2*p* hybridization from O *K*-edge XAS of structurally similar perovskites having formula of $AA'BB'O_3$ (A and A′ are rare-earth and/or alkaline earth metals, B and B′ are 3*d* transition metals, and O is oxygen). We apply a similar approach that was reported by de Groot et al. on structurally similar perovskite model compounds. Although several studies have examined the influence of A-site and B-site substitution on the degree of mixing between O 2*p* and transition metal 3*d* states, such as through the $La_{1-x}Sr_xMnO_{3-\delta}$[16] and $LaNi_xMn_{1-x}O_3$ series, systematic studies of hybridization in the perovskites of the first-row transition metal series examining the influence of *d*-electron, valency, and A-site substitution have not been reported. In this work, we first explored different methods for assessing trends in hybridization from the O *K*-edge spectra using isovalent $LaBO_3$ (B = Cr, Mn, Fe, Co, Ni) oxides as a model system. Density functional theory (DFT) calculations were used to verify the trends established and support the analysis employed. We then extended the analysis to examine the influence of different B-site valence states and different A-site ions. We conclude by demonstrating that the hybridization analysis can be used to explore interesting oxide phenomena, specifically drawing correlations between the metal−oxygen hybridization and activity for the oxygen evolution reaction (OER) in basic solution.

EXPERIMENTAL SECTION

O *K*-edge X-ray absorption spectra were collected at Saga-LS (BL-12), Japan, the Advanced Light Source (ALS) at the Lawrence Berkeley National Laboratory (Beamline 8.0.1), and the Advanced Photon Source (APS) at the Argonne National Laboratory (Beamline 4-ID-C). The measurements were collected in the total-electron-yield mode at $\sim 10^{-9}$ Torr (corresponding to a typical probe depth of less than 10 nm penetration depth[20]). The fluorescence yield signals were collected through photon detection mode of Channeltron detectors with a probe depth of approximately 100 nm. All spectra were normalized to the absorption background at the energy ranges both below the absorption edge and at ∼570 eV. All samples used in this study were characterized by X-ray diffraction to determine phase purity. The synthesized materials all had a single phase except the $LaNiO_{3-\delta}$, where <2% of NiO was present. Experimental details on the synthesis can be found in the Supporting Information.

Stoichiometric $ANiO_3$ (A = La, Pr, Nd, Sm, Eu, and Gd), studied at the APS, were synthesized under 600 bar oxygen pressure at 1080 °C as described previously.[21,22] For the stoichiometric samples, the oxygen contents were verified by thermogravimetric analysis to be 3.00 ± 0.01.

RESULT AND DISCUSSION

I. Influence of *d*-Electron Number. The results of the total-electron-yield O *K*-edge spectra of $LaBO_3$ (B = Cr, Mn, Fe, Co, and Ni) powders are shown in Figure 1. Our results

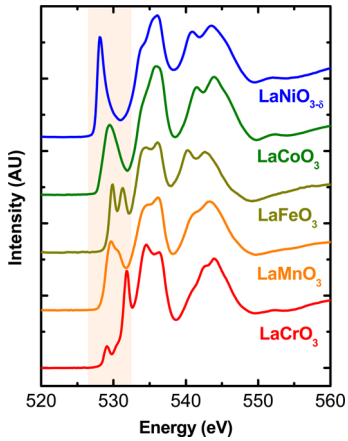

Figure 1. O *K*-edge X-ray absorption spectra of $LaBO_3$ (B = Cr, Mn, Fe, Co, Ni). The shaded region centered at ∼530 eV represents the feature assigned to O 1*s* excitation to the B 3*d*−O 2*p* hybridized state. Spectra were collected in electron yield mode at room temperature.

have similar features to the spectra of perovskites reported in the literature,[16,23−25] although it should be noted that the $LaCrO_3$ data shows a small peak feature ∼529 eV that has not been observed previously.[26] In general, the first peak (∼530 eV) corresponds to the excitation from the O 1*s* state to the hybridized O 2*p*−B 3*d* state, and the second (∼535 eV) and third peaks (∼543 eV) have been attributed to the excitations of O 1*s* to O 2*p*−La 5*d*, and O 2*p*−B 4*sp*, respectively. Unlike the second and third features, which remain largely unchanged with first row transition metal substitution, the first feature undergoes significant transformations in both shape and peak energy going from Cr to Ni. This observation is expected as the second feature corresponds to the La 5*d* state (centered about ∼535 eV), which is formally identical for all of the $LaBO_3$ samples, and the third feature corresponds to the transition metal 4*sp* state (centered about ∼545 eV), which generally has a wider bandwidth and therefore is largely similar across different B transition metals.

We employ the first feature of the O *K*-edge spectra to assess the extent of the B 3*d*−O 2*p* hybridization[15] among different 3*d* transition metals. We show that the hybridization parameter increases with the nominal number of *d*-electrons for transition metal ions in a nominal 3+ valency using three parametrizations of hybridization, as shown in Figure 2. First, we assume the simplest form of hybridization, whereby all of the O 2*p*−B 3*d* states, occupied and unoccupied, have the same extent of hybridization. Under this assumption, the spectral intensity is linearly proportional to the product of the total number of the empty O 2*p*−B 3*d* state and their extent of hybridization. The hybridization can be related to the spectral intensity using hybridization $\propto(1/h_{3d})\cdot I$. Here, I is the background-corrected spectral intensity of the O 1*s* to O 2*p*−B 3*d* excitation of the O *K*-edge spectra, and h_{3d} is the total number of empty O 2*p*−B 3*d* states per unit cell, which amounts to the nominal number of empty B 3*d* levels in both e_g and t_{2g} symmetry (h_{e_g} and $h_{t_{2g}}$). We henceforth refer to h_{3d} as $h_{e_g} + h_{t_{2g}}$. We extract the intensity of the excitation by first removing a linear background between the two nearest local minima to correct for the background absorption, then integrate the area underneath (see Figure S1, in Supporting Information).[13] As shown in Figure 2A, we found the hybridization parameter to *increase* with the nominal number of *d*-electrons for transition metal ions in 3+ valency.

dx.doi.org/10.1021/jp410644j | J. Phys. Chem. C 2014, 118, 1856−1863

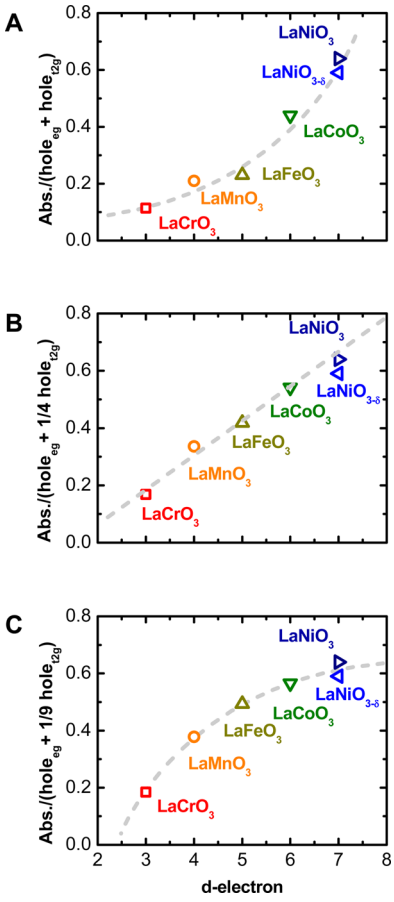

Figure 2. Evolution of the hybridization parameter for $LaBO_3$ with the *d*-electron number. The extent of hybridization is shown for various normalizations. (A) Intensity normalized by the total number of empty B 3*d* states, Abs./(hole$_{e_g}$ + hole$_{t_{2g}}$). (B) Normalization based on twice the hybridization for e_g symmetry states over t_{2g} (i.e., $T_\sigma = 2T_\pi$), resulting in Abs./(hole$_{e_g}$ + 1/4 hole$_{t_{2g}}$). (C) Normalization based on thrice the hybridization of e_g symmetry states over t_{2g} (i.e., $T_\sigma = 3T_\pi$), resulting in Abs./(hole$_{e_g}$ + 1/9 hole$_{t_{2g}}$). The absorbance was taken from the first feature of the O *K*-edge spectra (shaded region in Figure 1), corrected with a linear background. The dashed gray lines serve only as a visual guide to the trend.

We briefly discuss the errors associated with this analysis. The first source of error comes from the synchrotron's intensity variation. As we limit our comparison to samples collected in the same synchrotron and using the same reference, this contribution to the error is negligible and largely unimportant for the data shown here. We discuss this in more detail later in the text. The second error contribution comes from the normalization of the spectra. The methodology used for analysis is the conventional method for normalization, which assumes that the inelastic scattering background of O *K*-edge scales is not chemistry-specific. Because we have selected the same normalization energy (~570 eV) for all compounds, this error is small. The final error contribution comes from the analysis and is likely the largest source of error. We assume that the error is mainly generated by the local minima fit, which was estimated to be less than 3% by comparing the result against multiple integrations of the same spectra, with small fluctuations in the selection of boundary conditions. This is smaller than the size of the data points in this Article and we thus exclude error bars in our figures.

To improve the accuracy of our assumption, we take into account the possibility that the transfer integral associated with the e_g symmetry states is approximately 2-fold stronger than that of t_{2g} states owing to the angular overlap with the ligand field, which would lead to holes in the t_{2g} states contributing ~4 times less to the O *K*-edge spectral intensity than holes in the e_g states. This assumption is based on previous works that have suggested that the 3*d* states with e_g symmetry (σ-interaction) can have a different extent of hybridization with O 2*p* states than the 3*d* states in t_{2g} symmetry (π-interaction)[10,15,27] resulting in a transfer integral ratio of ~2 (i.e., $T_\sigma \approx 2T_\pi$).[27] This second parametrization of the extent of hybridization, whereby hybridization $\propto I/(h_{e_g} + (1/4)h_{t_{2g}})$, was found to increase with the *d*-electron number in a linear fashion, as shown in Figure 2B. The same trend can also be obtained when assuming the transfer integral with the e_g states is ~3 times stronger than that of t_{2g} states, that is, holes in the t_{2g} states contribute ~9 times less than holes in the e_g states to the O *K*-edge spectral intensity (Figure 2C). The systematic appearance of this trend independent of the weighting between e_g and t_{2g} states suggests that the number of *d*-electrons trends with increasing hybridization across isovalent transition metal compounds.

To further support the validity of our analysis, we used first-principles density functional theory within the Generalized Gradient Approximation (GGA) plus Hubbard formalism (GGA+U) to calculate the B 3*d*- and O 2*p*-projected density of states (DOS). Additional details on the DFT calculations can be found in the Supporting Information.

The O 2*p*−B 3*d* hybridized ground states that correspond with the O *K*-edge X-ray absorption prepeaks can be approximated by single-particle O 2*p*-projected DOS, and lie in the first 5 eV above the Fermi level of the $LaBO_3$ oxides (shaded region in Figure 3A). Good agreement can be seen between the calculated DOS and the O *K*-edge prepeak features, where the reduction in the number of features in the experimental data may result primarily from experimental broadening (e.g., instrumental broadening and core-hole lifetime broadening) and final-state effects (e.g., Coulombic interactions with the core-hole and multiplet splitting). Such similarity between the O *K*-edge X-ray absorption spectrum and O 2*p* density of states has been observed previously in TMOs such as $LiCoO_2$.[28] However, it should be emphasized that the comparison presented here with the DFT-computed DOS is a rough approximation which serves to capture the trends in hybridization rather than provide a quantitative comparison with the XAS results, as excited states and quasi-particle effects are beyond the capabilities of ground state DFT. By determining the degree of hybridization from the integrated O 2*p*−B 3*d* unoccupied DOS (first 5 eV above the Fermi level) and normalizing under the assumption that the transfer integrals for e_g-symmetry states and t_{2g}-symmetry states differ by a factor of 2 ($T_\sigma = 2T_\pi$), we again find a linear relationship between the metal−oxygen hybridization and the *d*-electron number that strongly resembles the experimental trend (Figure 3B). The good agreement between theory and experiment suggests that normalizing the integrated area under the O *K*-edge prepeak can provide a reliable method for comparing metal−oxygen hybridization among compounds.

We compare our finding that the hybridization increases with the *d*-electron number against the previous literature results, where hybridization is defined to be the ratio between the

dx.doi.org/10.1021/jp410644j | J. Phys. Chem. C 2014, 118, 1856−1863

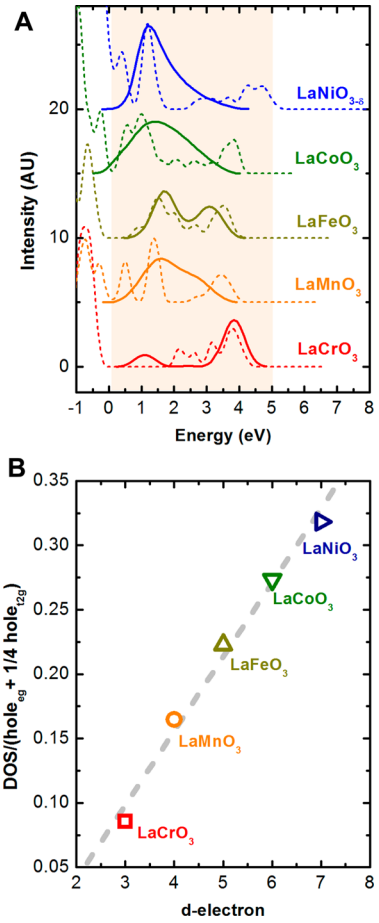

Figure 3. Comparison of DFT calculated O 2*p* unoccupied density of states with the O *K*-edge XAS for $LaBO_3$ compounds. (A) DFT calculations (dashed lines) of the O 2*p*-projected density of states in the first 5 eV above the Fermi level (shaded), which are hybridized with B 3*d* states. Spectral weighting of the O *K*-edge XAS spectra after linear background subtraction (solid lines) show good agreement with the DFT calculations (aligned to the DFT Fermi level by matching the centroid of the two data sets). (B) Linear trend in hybridization computed from the integrated O 2*p* unoccupied density of states associated with O 2*p*−B 3*d* hybridization, normalized assuming $T_\sigma = 2T_\pi$. The dashed gray line serves only as a visual guide to the trend.

transfer integral (T) and the charge-transfer energy (Δ), approximated as the energy difference between the unoccupied 3*d* and the O 2*p* levels.[29,30] Based on this definition, our experimental result agrees with the previous experimental results in the case of binary oxides (TiO, CrO, MnO, FeO, and NiO) and ternary oxides ($LaTiO_3$, $LaCrO_3$, $LaMnO_3$, and $LaFeO_3$) reported by Bocquet and co-workers.[18,31] In these studies, the hybridization, estimated to scale with the ratio of the ($pd\sigma$) overlap integral to the charge-transfer energy Δ, increases with the *d*-electron number due to vanishing Δ. We note that the ($pd\sigma$) integral also changes with respect to number of *d*-electrons; however, the change is lower in magnitude compared to Δ.[19,31] This finding is not surprising as our experimental result follows the electronegativity trend for the B site in $LaBO_3$ systems.[10,32] Moving across the first-row transition metals to the right of the periodic table at fixed valence increases the transition metal electronegativity and brings the B 3*d* orbitals closer in energy to the O 2*p* orbitals, which results in increased covalent bonding and thereby stronger hybridization.

II. Influence of Valence. To probe the influence of valence on the hybridization, we examine the role of aliovalent Ca substitution for La in the series of $La_{1-x}Ca_xBO_3$ (where B = Cr, Mn, and Fe). The raw O *K*-edge spectra are shown in Figure 4A−C, where the unsubstituted $LaBO_3$ spectra of the same B

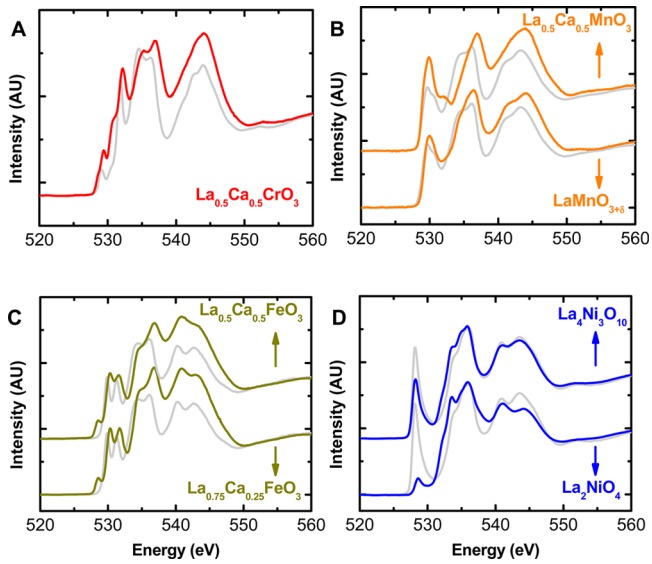

Figure 4. O *K*-edge X-ray absorption spectroscopy of $La_xCa_{1-x}BO_3$ and $La_{n+1}Ni_nO_{3n+1}$: (A) $La_{0.5}Ca_{0.5}CrO_3$, $LaCrO_3$ is shown in gray as a reference; (B) $La_{0.5}Ca_{0.5}MnO_3$ and $LaMnO_{3+\delta}$, $LaMnO_3$ is shown in gray; (C) $La_{0.5}Ca_{0.5}FeO_3$ and $La_{0.75}Ca_{0.25}FeO_3$, $LaFeO_3$ is shown in gray; (D) $La_4Ni_3O_{10}$ and La_2NiO_4, $LaNiO_3$ is shown in gray.

transition metal are displayed in gray lines as reference. With Ca-substitution, all three features of the spectra change significantly, in agreement with previous literature reports on the similar divalent case of Sr substitution.[16,24,26] This is a result of the fact that Ca substitution (of La) can serve as an electron acceptor, which oxidizes the transition metal and manifests as a change in the final state of the O *K*-edge excitation to both the A-site (chemical substitution) and the B-site (oxidation). As our interest is in the B 3*d*−O 2*p* hybridization, we again focus on the first feature which corresponds to the excitation to the hybridized B 3*d*−O 2*p* state. We perform the same form of analysis as in Figure 2B, assuming that the e_g transfer integral is twice that of the t_{2g}, to assess the hybridization trend of these B-site substituted compounds. We note again that the analysis based on assuming that the e_g transfer integral is the same or thrice that of the t_{2g} would yield the same trends and hence are not shown. As we are interested in how the relative change in the valency can influence the hybridization, we compare the extracted degree of hybridization against the parent trivalent $LaBO_3$ compound. In other words, we normalize all of the extracted hybridization parameters with respect to the extracted hybridization parameter of the unsubstituted $LaBO_3$. The result of this comparison is shown in Figure 5. We find that hybridization generally increases with Ca substitution, suggesting that hybridization generally increases with the nominal B oxidation state.

To further verify the influence of the cation oxidation state on hybridization, we also examined compounds in the $La_{n+1}Ni_nO_{3n+1}$ series. The O *K*-edge spectra of $La_4Ni_3O_{10}$ (nominally $Ni^{2.7+}$) and La_2NiO_4 (nominally Ni^{2+}) are compared with that of $LaNiO_3$ (nominally Ni^{3+}) O *K*-edge in Figure 4D.

dx.doi.org/10.1021/jp410644j | J. Phys. Chem. C 2014, 118, 1856−1863

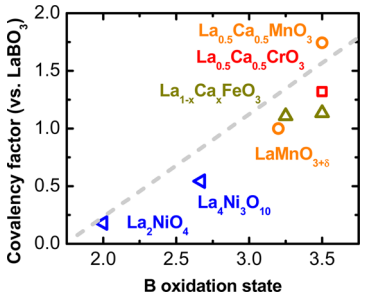

Figure 5. Evolution of covalency with respect to different B oxidation states using $La_{1-x}Ca_xBO_3$ and $La_{n+1}Ni_nO_{3n+1}$ as model compounds. The covalency enhancement factor is calculated from a ratio of the hybridization parameter of either $La_{1-x}Ca_xBO_3$ or $La_{1+x}NiO_{3+x}$ with respect to the parent $LaBO_3$ compound.

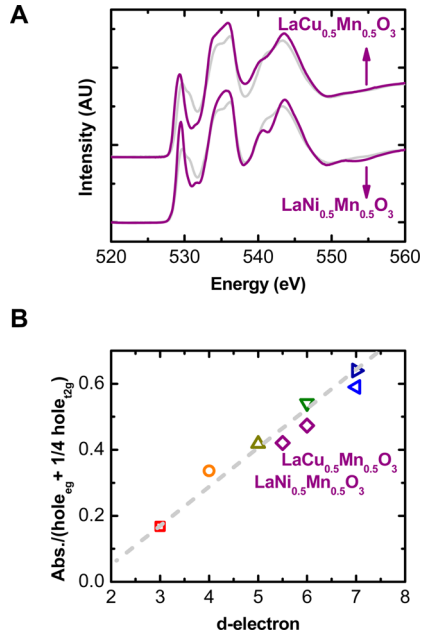

Figure 6. O *K*-edge X-ray absorption spectra of $LaBB'O_3$ (BB′ = $Cu_{0.5}Mn_{0.5}$ and $Ni_{.5}Mn_{0.5}$): (A) Raw spectra, The gray lines show a $LaMnO_3$ O *K*-edge reference; (B) $LaBB'O_3$ covalency parameter vs *d*-electron count, with $LaBO_3$ data as references, the gray line serves only as guide to the trend.

These Ruddlesden−Popper phases (Ni^{2+} and $Ni^{2.7+}$) were found to have lower hybridization than the parent $LaNiO_3$ (Ni^{3+}) compound (Figure 4), in agreement with the trend we observed in the $La_{1-x}Ca_xBO_3$ case, whereby increasing oxidation state leads to increasing hybridization.

We explain the relationship between the hybridization and the transition metal valence state as changes in Δ with the oxidation state. More specifically, lowering of the transition metal 3*d* level due to oxidation reduces the gap between the transition 3*d* level and the O 2*p*, resulting in smaller Δ.[18] As the hybridization is estimated by the ratio between the transfer integral and Δ, decreasing Δ due to higher transition metal oxidation state causes the hybridization to increase with the transition metal valency. We thus propose that the trend for the $La_{n+1}Ni_nO_{3n+1}$ and the $La_{1-x}Ca_xBO_3$ hybridizations follow the change in Δ, whereby increasing oxidation state consequently increases the hybridization. The implication of our result is that, within the limit of the oxo-perovskites, the hybridization behavior can be tuned by the choice of both the B-site transition metal and the oxidation state.

III. Influence of Mixed B-Site. We further examine the role of B-site partial substitution on the hybridization. The O *K*-edge spectra of $LaNi_{0.5}Mn_{0.5}O_3$ and $LaCu_{0.5}Mn_{0.5}O_3$ are compared with that of $LaMnO_3$ (shown in gray) in Figure 6A. Notably, the first peak due to the excitation of the O 1*s* to empty O 2*p* and B 3*d* states changes significantly with B-site substitution, reflecting the changes in both the extent of the B 3*d*−O 2*p* hybridization and the nominal number of empty B 3*d*−O 2*p* state. To assess the hybridization parameter, we perform the same analysis as in the above section. We found that the observed trend is consistent with the assumption that the hybridization of Ni−Mn and Cu−Mn compounds can be approximated by the average *d*-electron of the two transition metals (Figure 6B). In the context of the molecular orbital approach, the center of the constituent B 3*d* states is approximately determined by the weighted average of the relative density of states for the constituent transition metal ion 3*d* bands, which should scale with the ratio of the transition metal ions. Thus, averaging the hybridization accounts for the shift in the 3*d*-band center induced by introducing additional 3*d* states of different energy. It is relevant to note that the Ni/Cu valence may be reduced from its original trivalent state, which may affect the hybridization,[13,33] as shown in the above section. However, such a change is offset by the Mn valence, which must be oxidized to preserve charge neutrality.

IV. Influence of the Detection Mode. In this section, we focus on the difference in using the total-electron-yield mode (which typically has an information depth of less than 10 nm) and the fluorescence-yield mode (which has probing depth of approximately 100 nm). Our interest in studying this effect is driven by the recent suggestion that $LaCoO_3$ can have intermediate spin state at the surface but low spin states in the bulk.[34] Furthermore, we are interested in understanding the validity of applying surface-sensitive photoemission techniques to examine the TMO hybridization. To examine how the hybridization evolves from bulk to surface, we perform the same analysis for both electron-yield and fluorescence-yield O *K*-edge XAS spectra. A comparison between the electron-yield data from Saga, which are used in the analysis of Figures 1−6, and fluorescence-yield data from ALS are shown in Figure 7A−C for $LaNiO_{3-\delta}$, $LaCoO_3$, and $LaFeO_3$. We apply the same analysis that was developed earlier in this manuscript (Figure 7D). Interestingly, while the hybridization in bulk is generally higher than that at the surface, which could be attributed to the self-absorption effect in fluorescence signals, the trends with *d*-electron for both bulk and surface hybridization are consistent with one another. It should be noted that in this analysis we have assumed identical spin states at the surface and in the bulk for $LaFeO_3$ and $LaNiO_{3-\delta}$, and bulk low spin state ($t_{2g}^6e_g^0$) and surface intermediate spin state ($t_{2g}^5e_g^1$) for $LaCoO_3$.[34] To ensure that this observation is not due to the instrumental variation between different synchrotrons, we also measured the electron-yield spectra at ALS for comparison. We find that the difference in the estimated hybridization based on the electron-yield data collected from Saga and ALS is within 10%, and hence, we assume this reflects the intrinsic error from the synchrotron difference. The observed trend, whereby hybridization increases with increasing *d*-electron count, can be observed in both the electron-yield and the fluorescence-yield mode and thus the trend is not detection-mode-specific. This observation suggests that the hybridization trend is comparable for both surface and bulk and largely originates from the nature

dx.doi.org/10.1021/jp410644j | J. Phys. Chem. C 2014, 118, 1856−1863

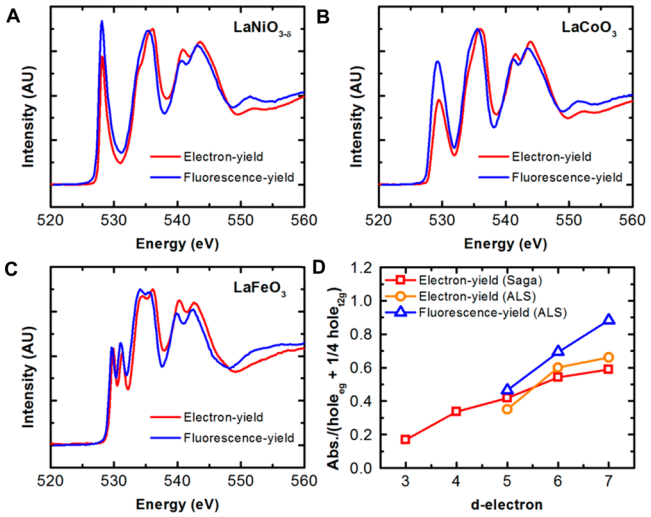

Figure 7. Comparison between electron-yield and fluorescence-yield O *K*-edge XAS. Spectra collected in the electron- and the fluorescence-yield mode of (A) $LaNiO_{3-\delta}$, (B) $LaCoO_3$, and (C) $LaFeO_3$. (D) Calculated covalency parameters from both spectra. For $LaCoO_3$, low spin ($t_{2g}^6e_g^0$) is assumed for the bulk (fluorescence-yield), whereas intermediate spin ($t_{2g}^5e_g^1$) is assumed for the surface (electron yield).

of the transition metal *d*-state. Practically, this finding validates that either fluorescence-yield or electron-yield analysis could be used for assessing the hybridization trend for perovskite oxides.

V. Influence of A-Site Substitution. We use the fluorescence O *K*-edge data to examine the role of A-site ions on the hybridization of $ANiO_3$ (A = La, Pr, Nd, $Nd_{0.5}Sm_{0.5}$, Sm, Eu, Gd, Figure 8A). Interestingly, we find stoichiometric

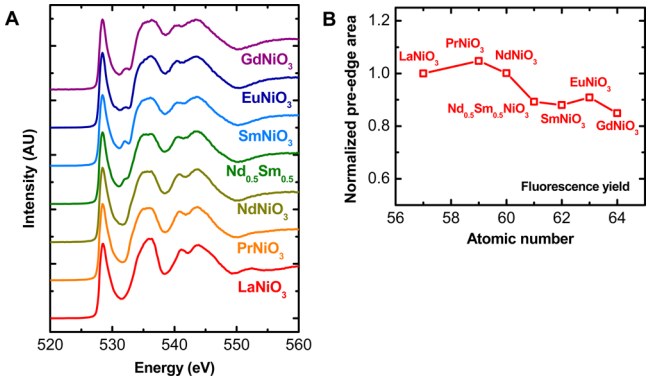

Figure 8. Effect of A-site substitution on the hybridization of stoichiometric $ANiO_3$. (A) X-ray absorption spectra of $ANiO_3$. (B) Pre-edge O *K*-edge area of $ANiO_3$ as A-site atomic number. All XAS was collected in fluorescence-yield mode.

$LaNiO_3$ to have slightly higher hybridization than non-stoichiometric $LaNiO_{3-\delta}$, although the difference is within the experimental error (Figure 2). Comparing $ANiO_3$ across the different A-substitution (Figure 8B), we find nonmonotonic decrease in the pre-edge area (and hence hybridization, as all $ANiO_3$ compounds have the same nominal Ni^{3+} with $t_{2g}^6e_g^1$ configuration). We note that the difference across the A-site substitution is small relative to B-site substitution. This finding is not too surprising as the hybridization difference between $ANiO_3$ is driven by the Ni−O bond angle, which controls bandwidth.[21,22,35] This is in contrast to B-site substitution, where the charge-transfer gap controls the electronegativity as shown in the earlier section. We therefore conclude that the hybridization is not significantly influenced by the choice of the A-site substitution, provided that the transition metal oxidation state remains the same and the structural component (bond angle) plays a less significant role in the hybridization than the difference between the Ni 3*d* and the O 2*p* energy levels.

VI. Influence of the Hybridization on the Oxygen Electrocatalysis. We have previously demonstrated that increasing hybridization can lead to increased oxygen electrocatalysis. This argument is driven by the need to inject/extract electrons from oxygen during oxygen electrocatalysis. Increasing character of the O 2*p* near the Fermi level can promote this injection/extraction by allowing the B 3*d* state to mix with the oxygen (B^{3+}-O^{2-} ↔ $B^{(3+\delta)+}$-$O^{(2-\delta)-}$). To demonstrate this point, we measured the OER activity of stoichiometric $LaNiO_3$ and assess its performance using the standard three electrode cell configuration. The result of the OER activity of this material is compared against the results of $LaMnO_3$, $LaCoO_3$, and $LaNiO_{3-\delta}$ that were reported previously.[14] Note that we choose these four materials as they have ∼1 e_g electron, a condition that is required for high OER performance.[14] Applying the method to extract the hybridization parameter as shown above, we found that increasing hybridization can further increase the OER activity (Figure 9), which is consistent

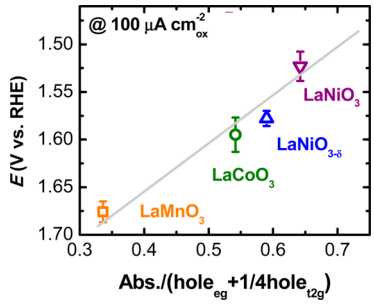

Figure 9. Increasing covalency with stoichiometric $LaNiO_3$ for catalysis application. Influence of covalency on the oxygen evolution activity of $LaNiO_3$, compared against other compounds with approximate unity e_g. All XAS was collected in an electron-yield mode. Spectra for $LaMnO_3$, $LaCoO_3$, and $LaNiO_{3-\delta}$ were collected at Saga, whereas $LaNiO_3$ was collected at ANL.

with our previous result suggesting the critical role of hybridization for oxygen electrocatalysis.[13,14] Our finding in this work thus suggests that designing TMO with higher hybridization for oxygen evolution should focus on finding compounds with increased B−O interaction by altering the electronic or chemical nature of the B-site rather than the A-site.

■ CONCLUSIONS

We show that the hybridization increases with *d*-electron number for $LaBO_3$ (B = Cr, Mn, Fe, Co, Ni) compounds, which can be attributed to the increasing electronegativity of the transition metal as *d*-electron number increases. Our finding is consistent with the results from literature, where the charge-transfer energy decreases with *d*-electron.[18,19] We further report that hybridization increases with the increasing oxidation state of B transition metal ions based on combined studies on Ca substitution and Ruddlesden−Popper phases. This effect can be explained by reduction in the charge transfer energy with increasing oxidation state. We further demonstrate that bulk

dx.doi.org/10.1021/jp410644j | J. Phys. Chem. C 2014, 118, 1856−1863

hybridization follows similar trends to surface hybridization. We assess the influence of lanthanide on the $ANiO_3$ hybridization and find that the influence of the choice of A-site on the hybridization of the Ni 3*d*−O 2*p* states is much less than that of B-site substitution and valency change. Lastly, we confirm the role of the hybridization on the oxygen evolution activity, a result of which suggests increasing hybridization is key to design of future water-splitting catalyst.

■ ASSOCIATED CONTENT

Supporting Information

Details for oxide synthesis and DFT experimental methods. This material is available free of charge via the Internet at http://pubs.acs.org.

■ AUTHOR INFORMATION

Corresponding Author

*E-mail: jsuntivich@cornell.edu; shaohorn@mit.edu.

Present Address

[§]Department of Materials Science and Engineering, Cornell University, Ithaca, NY 14850, United States (J.S.).

Notes

The authors declare no competing financial interest.

■ ACKNOWLEDGMENTS

This work was supported in part by DOE Basic Energy Science (SISGR DE-SC0002633), by the DOE Hydrogen Initiative Program under Award No. DE-FG02-05ER15728, and Toyota Motor Company. J.S. was supported in part by the Chesonis Foundation Fellowship (MIT) and the Ziff Environmental Fellowship (Harvard). J.B.G was supported by the Robert A. Welch Foundation, Houston, TX. J.M.R. acknowledges funding from ARO (W911NF-12-1-0133). We thank Alexis Grimaud, Kevin J. May, Kelsey A. Stoerzinger, Paul Olalde-Velasco, and Naoaki Yabuuchi for their help with the experimental measurements. The Advanced Light Source is supported by the Director, Office of Science, Office of Basic Energy Sciences, of the U.S. Department of Energy under Contract No. DE-AC02-05CH11231. Work at the Advanced Photon Source is supported by the U.S. Department of Energy, Office of Basic Energy Sciences under Contract No. DE-AC02-06CH11357.

■ REFERENCES

(1) Goodenough, J. B. Electronic and Ionic Transport Properties and Other Physical Aspects of Perovskites. *Rep. Prog. Phys.* **2004**, *67*, 1915−1993.

(2) Goodenough, J. B.; Kim, Y. Challenges for Rechargeable Li Batteries. *Chem. Mater.* **2010**, *22*, 587−603.

(3) Marianetti, C. A.; Kotliar, G.; Ceder, G. Role of Hybridization in Na_xCoO_2 and the Effect of Hydration. *Phys. Rev. Lett.* **2004**, *92*.

(4) Arima, T.; Tokura, Y.; Torrance, J. B. Variation of Optical Gaps in Perovskite-Type 3*d* Transition-Metal Oxides. *Phys. Rev. B* **1993**, *48*, 17006−17009.

(5) Maiti, K. Role of Covalency in the Ground-State Properties of Perovskite Ruthenates: A First-Principles Study Using Local Spin Density Approximations. *Phys. Rev. B* **2006**, *73*.

(6) Van Aken, B. B.; Palstra, T. T. M.; Filippetti, A.; Spaldin, N. A. The Origin of Ferroelectricity in Magnetoelectric $YMnO_3$. *Nat. Mater.* **2004**, *3*, 164−170.

(7) Mannhart, J.; Schlom, D. G. Oxide Interfaces: An Opportunity for Electronics. *Science* **2010**, *327*, 1607−1611.

(8) Takaobushi, J.; Ishikawa, M.; Ueda, S.; Ikenaga, E.; Kim, J. J.; Kobata, M.; Takeda, Y.; Saitoh, Y.; Yabashi, M.; Nishino, Y.; et al. Electronic Structures of $Fe_{3-x}M_xO_4$ (M = Mn, Zn) Spinel Oxide Thin Films Investigated by X-ray Photoemission Spectroscopy and X-ray Magnetic Circular Dichroism. *Phys. Rev. B* **2007**, *76*.

(9) Shimakawa, Y.; Kubo, Y.; Hamada, N.; Jorgensen, J. D.; Hu, Z.; Short, S.; Nohara, M.; Takagi, H. Crystal Structure, Magnetic and Transport Properties, and Electronic Band Structure of $A_2Mn_2O_7$ Pyrochlores (A = Y, In, Lu, and Tl). *Phys. Rev. B* **1999**, *59*, 1249−1254.

(10) Goodenough, J. B. Covalency Criterion for Localized vs Collective Electrons in Oxides with the Perovskite Structure. *J. Appl. Phys.* **1966**, *37*, 1415−&.

(11) Chakhalian, J.; Freeland, J. W.; Habermeier, H. U.; Cristiani, G.; Khaliullin, G.; van Veenendaal, M.; Keimer, B. Orbital Reconstruction and Covalent Bonding at an Oxide Interface. *Science* **2007**, *318*, 1114−1117.

(12) Chakhalian, J.; Rondinelli, J. M.; Liu, J.; Gray, B. A.; Kareev, M.; Moon, E. J.; Prasai, N.; Cohn, J. L.; Varela, M.; Tung, I. C.; et al. Asymmetric Orbital-Lattice Interactions in Ultrathin Correlated Oxide Films. *Phys. Rev. Lett.* **2011**, *107*.

(13) Suntivich, J.; Gasteiger, H. A.; Yabuuchi, N.; Nakanishi, H.; Goodenough, J. B.; Shao-Horn, Y. Design Principles for Oxygen Reduction Activity on Perovskite Oxide Catalysts for Fuel Cells and Metal-Air Batteries. *Nat. Chem.* **2011**, *3*, 546−550.

(14) Suntivich, J.; May, K. J.; Goodenough, J. B.; Gasteiger, H. A.; Shao-Horn, Y. A Perovskite Oxide Optimized for Oxygen Evolution Catalysis from Molecular Orbital Principles. *Science* **2011**, *334*, 1383−1385.

(15) de Groot, F. M. F.; Grioni, M.; Fuggle, J. C.; Ghijsen, J.; Sawatzky, G. A.; Petersen, H. Oxygen 1*s* X-ray-Absorption Edges of Transition-Metal Oxides. *Phys. Rev. B* **1989**, *40*, 5715−5723.

(16) Abbate, M.; Degroot, F. M. F.; Fuggle, J. C.; Fujimori, A.; Strebel, O.; Lopez, F.; Domke, M.; Kaindl, G.; Sawatzky, G. A.; Takano, M. Controlled-Valence Properties of $La_{1-x}Sr_xFeO_3$ and $La_{1-x}Sr_xMnO_3$ Studied by Soft-X-Ray Absorption-Spectroscopy. *Phys. Rev. B* **1992**, *46*, 4511−4519.

(17) Kuiper, P.; Kruizinga, G.; Ghijsen, J.; Grioni, M.; Weijs, P. J. W.; Degroot, F. M. F.; Sawatzky, G. A.; Verweij, H.; Feiner, L. F.; Petersen, H. X-ray Absorption Study of the O 2*p* Hole Concentration Dependence on O Stoichiometry in $YBa_2Cu_3O_x$. *Phys. Rev. B* **1988**, *38*, 6483−6489.

(18) Bocquet, A. E.; Mizokawa, T.; Saitoh, T.; Namatame, H.; Fujimori, A. Electronic Structure of 3*d*-Transition-Metal Compounds by Analysis of the 2*p* Core-Level Photoemission Spectra. *Phys. Rev. B* **1992**, *46*, 3771−3784.

(19) Saitoh, T.; Bocquet, A. E.; Mizokawa, T.; Fujimori, A. Systematic Variation of the Electronic-Structure of 3*d* Transition-Metal Compounds. *Phys. Rev. B* **1995**, *52*, 7934−7938.

(20) Abbate, M.; Goedkoop, J. B.; Degroot, F. M. F.; Grioni, M.; Fuggle, J. C.; Hofmann, S.; Petersen, H.; Sacchi, M. Probing Depth of Surface X-ray Absorption Spectroscopy Measured in Total Electron-Yield-Mode. *Surf. Interface Anal.* **1992**, *18*, 65−69.

(21) Zhou, J. S.; Goodenough, J. B.; Dabrowski, B.; Klamut, P. W.; Bukowski, Z. Probing the Metal-Insulator Transition in Ni(III)-Oxide Perovskites. *Phys. Rev. B* **2000**, *61*, 4401−4404.

(22) Zhou, J. S.; Goodenough, J. B.; Dabrowski, B.; Klamut, P. W.; Bukowski, Z. Enhanced Susceptibility in $LNiO_3$ Perovskites (L = La, Pr, Nd, $Nd_{0.5}Sm_{0.5}$). *Phys. Rev. Lett.* **2000**, *84*, 526−529.

(23) Medarde, M.; Fontaine, A.; Garciamunoz, J. L.; Rodriguezcarvajal, J.; Desantis, M.; Sacchi, M.; Rossi, G.; Lacorre, P. $RNiO_3$ Perovskites (R = Pr,Nd): Nickel Valence and the Metal-Insulator Transition Investigated by X-ray-Absorption Spectroscopy. *Phys. Rev. B* **1992**, *46*, 14975−14984.

(24) Toulemonde, O.; N'Guyen, N.; Studer, F.; Traverse, A. Spin State Transition in $LaCoO_3$ with Temperature or Strontium Doping as seen by XAS. *J. Solid State Chem.* **2001**, *158*, 208−217.

(25) Abbate, M.; Fuggle, J. C.; Fujimori, A.; Tjeng, L. H.; Chen, C. T.; Potze, R.; Sawatzky, G. A.; Eisaki, H.; Uchida, S. Electronic Structure and Spin-State Transition of $LaCoO_3$. *Phys. Rev. B* **1993**, *47*, 16124−16130.

(26) Sarma, D. D.; Maiti, K.; Vescovo, E.; Carbone, C.; Eberhardt, W.; Rader, O.; Gudat, W. Investigation of Hole-Doped Insulating $La_{1-x}Sr_xCrO_3$ by Soft-X-ray Absorption Spectroscopy. *Phys. Rev. B* **1996**, *53*, 13369−13373.
(27) Mizokawa, T.; Fujimori, A. Electronic Structure and Orbital Ordering in Perovskite-Type 3*d* Transition-Metal Oxides Studied by Hartree-Fock Band-Structure Calculations. *Phys. Rev. B* **1996**, *54*, 5368−5380.
(28) Juhin, A.; De Groot, F. M. F. Angular Dependence of Core Hole Screening in $LiCoO_2$: A DFT+U Calculation of the Oxygen and Cobalt *K*-Edge X-ray Absorption Spectra. *Phys. Rev. B* **2010**, *81*, 115115.
(29) Goodenough, J. B. Jahn-Teller Phenomena in Solids. *Annu. Rev. Mater. Sci.* **1998**, *28*, 1−27.
(30) Goodenough, J. B. First-Order Changes in Ionic/Covalent Bonding. *Ferroelectrics* **1992**, *130*, 77−86.
(31) Bocquet, A. E.; Mizokawa, T.; Morikawa, K.; Fujimori, A.; Barman, S. R.; Maiti, K.; Sarma, D. D.; Tokura, Y.; Onoda, M. Electronic Structure of Early 3*d*-Transition-Metal Oxides by Analysis of the 2*p* Core-Level Photoemission Spectra. *Phys. Rev. B* **1996**, *53*, 1161−1170.
(32) Duffy, J. A. Ionic-Covalent Character of Metal and Nonmetal Oxides. *J. Phys. Chem. A* **2006**, *110*, 13245−13248.
(33) Sanchez, M. C.; Garcia, J.; Blasco, J.; Subias, G.; Perez-Cacho, J. Local Electronic and Geometrical Structure of $LaNi_{1-x}Mn_xO_{3+\delta}$ Perovskites Determined by X-ray-absorption Spectroscopy. *Phys. Rev. B* **2002**, *65*, 144409.
(34) Yan, J. Q.; Zhou, J. S.; Goodenough, J. B. Ferromagnetism in $LaCoO_3$. *Phys. Rev. B* **2004**, *70*, 014402.
(35) Torrance, J. B.; Lacorre, P.; Nazzal, A. I.; Ansaldo, E. J.; Niedermayer, C. Systematic Study of Insulator-Metal Transitions in Perovskites $RNiO_3$ (R = Pr, Nd, Sm, Eu) Due to Closing of Charge-Transfer Gap. *Phys. Rev. B* **1992**, *45*, 8209−8212.